

# Real-time label-free analysis of the thermostability of DNA structures using GelRed

Ya-Ya Hao<sup>1,2</sup> · Lei Liu<sup>2,3</sup> · Lu-Hao Zhang<sup>2</sup> · Qiu-Ling Huang<sup>2,3</sup> · Fei Wang<sup>2,3</sup> · Jiang Li<sup>2</sup> · Jia-Qiang Xu<sup>1</sup> · Li-Hua Wang<sup>2</sup>

Received: 15 March 2018 / Revised: 2 May 2018 / Accepted: 2 May 2018 / Published online: 28 August 2018  
© Shanghai Institute of Applied Physics, Chinese Academy of Sciences, Chinese Nuclear Society, Science Press China and Springer Nature Singapore Pte Ltd. 2018

**Abstract** In biological systems, conformational transformations of nucleic acids play critical roles in genetic regulation. However, it remains a tricky task to design and optimize specific labeling strategies to track these changes. In this study, we exploited an intercalating fluorescent dye, GelRed, to characterize different DNA structures. We studied the correlation between fluorescence intensity and DNA structural properties. We showed that single-stranded DNAs with predicted self-folded secondary structures show much stronger fluorescence than those without such structures. For double-stranded DNAs, we observed that fluorescence intensity is positively correlated to their GC

content. We also demonstrated that GelRed can be used to monitor DNA conformational changes upon temperature variations in real time. Based on these findings, we concluded that the fluorescence intensity of a GelRed-stained DNA structure has a good correlation with its thermostability in the form of a change in Gibbs free energy.

**Keywords** GelRed · Secondary structure · GC content · Conformational transformation

## 1 Introduction

In living organisms, conformational transformation of nucleic acids, especially genomic DNA, plays a vital role in genetic regulation and, thus, in biological functions such as growth and reproduction [1–6]. In the realm of DNA nanotechnology, a variety of nanodevices/nanomachines empowered by DNA conformational transformations have also been developed, showing great promise in smart theranostic applications [7–16]. Therefore, it is fundamentally important to develop methods for real-time monitoring of DNA conformational changes. In recent years, much progress has been made to develop fluorescence/luminescence platforms specifically responsive to structural alterations [17–23]. For example, dual-labeling strategies based on Förster fluorescence resonance energy transfer (FRET) have been widely exploited [24–27]. Because the FRET effect is highly sensitive to the spatial distance between labeled sites, one can obtain real-time information about conformational changes by monitoring the fluorescence variations resulting from FRET [28–30]. However, it remains a tricky task to choose proper sites on target structures for FRET labeling; thus, case-by-case

This work was supported by the National Natural Science Foundation of China (Nos. U1532119, 21775157, 21675167, and 31571014), and the Instrument Developing Project of the Chinese Academy of Sciences (Develop the Microsystems for Single Particle Tracking).

**Electronic supplementary material** The online version of this article (<https://doi.org/10.1007/s41365-018-0486-x>) contains supplementary material, which is available to authorized users.

- ✉ Jiang Li  
lijiang@sinap.ac.cn
- ✉ Jia-Qiang Xu  
xujiaqiang@shu.edu.cn
- ✉ Li-Hua Wang  
wanglihua@sinap.ac.cn

- <sup>1</sup> NEST Lab, Department of Chemistry, College of Science, Shanghai University, Shanghai 200444, China
- <sup>2</sup> Division of Physical Biology and Bioimaging Center, CAS Key Laboratory of Interfacial Physics and Technology, Shanghai Institute of Applied Physics, Chinese Academy of Sciences, Shanghai 201800, China
- <sup>3</sup> University of Chinese Academy of Sciences, Beijing 10049, China

optimization is often required to ensure the effectiveness of FRET responses [31].

On the other hand, fluorescent intercalating dyes, which emit fluorescence when intercalated into double helices of nucleic acids, provide a general and label-free way to characterize nucleic acid structures. For example, ethidium bromide (EtBr), a classic intercalating dye, has been routinely used in nucleic acid analysis applications, such as imaging of electrophoresis, assay of DNA damage in cells, and studies on interactions between DNA and drugs [32–36]. More recently, it has been used in detecting DNA mutations with the aid of graphene oxide [37] and in monitoring dynamic structural changes of DNA nanostructures [38]. Nevertheless, EtBr has been proven to be mutagenic by Ames tests [39] and is, thus, potentially harmful to its users and the environment.

GelRed is an updated version of EtBr. A GelRed molecule is composed of two EtBr molecules conjugated with a linker [40]. It shows higher sensitivity in nucleic acid characterization, while exhibiting much less genetic toxicity compared to EtBr. Thus, as a substitute to EtBr, GelRed has been widely used in qualitative and semi-quantitative analyses of nucleic acids [41–44]. However, as far as we know, there have been few studies on tracking conformational changes of DNA structures using GelRed.

Here, we used GelRed to characterize different DNA structures, including single-strand (ss-) DNAs with or without self-folded secondary structures and double-strand (ds-) DNA with different base compositions. We analyzed the fluorescence intensity from these GelRed-stained DNA structures. We also monitored the fluorescence dynamics of a DNA structure upon cyclic temperature variations. We found that the fluorescence intensity of a GelRed-stained DNA structure has a good correlation with its predicted Gibbs free energy, which can be utilized in studying DNA conformational changes.

## 2 Materials and methods

### 2.1 Materials

GelRed was purchased from Biotium. All ssDNAs were purchased from Sangon Biotech (Shanghai, China). Tris, EDTA-2Na·2H<sub>2</sub>O, and Mg(CH<sub>3</sub>COOH)<sub>2</sub>·4H<sub>2</sub>O were all purchased from Sinopharm Chemical Reagent Company (Beijing, China). The 20-bp DNA marker was purchased from Takara (Kusatsu, Japan).

### 2.2 Preparation and UV quantification DNA structures

The dsDNAs in this study were obtained by annealing complementary ssDNAs of equimolar amounts (1 μM) in 1 × TAE buffer, which were then heated to 95 °C and slowly cooled to 25 °C in 5.5 h. All the ssDNA was quantified using a UV-visible Spectrophotometer (Agilent Cary 100 Bio, Palo Alto, USA) with a dilution ratio of 100 in the 1 × TAE buffer [40 mM Tris, 2 mM EDTA-2Na·2H<sub>2</sub>O, and 12.5 mM Mg(CH<sub>3</sub>COOH)<sub>2</sub>·4H<sub>2</sub>O]; then, the molar concentration was calculated using the formula  $C = (A_{260} - A_{330})/(\epsilon \times M) \times D$ , where  $C$  is the molar concentration of ssDNA;  $A_{260}$  and  $A_{330}$  are the absorbance of DNA at the wavelength of 260 nm and 330 nm, respectively;  $\epsilon$  is the extinction coefficient of DNA;  $M$  is the molecular weight of the ssDNA; and  $D$  is the dilution ratio.

### 2.3 Fluorescence spectroscopy of GelRed-stained DNA

GelRed was diluted with 1 × TAE buffer to a working solution of 20 ×. Then, 90 μL of DNA structures of different concentrations was mixed with 10 μL 20 × GelRed working solution. The fluorescence was read immediately using a multi-mode microplate reader (Bio-Tek Synergy MX H1, USA) and fluorospectrophotometer (Edinburgh FS920, Livingston, Britain) with the excitation wavelength of 303 nm and the emission wavelength of 600 nm.

For temperature-dependent fluorescence dynamic analysis, the fluorescence intensity of the GelRed-stained DNA samples was monitored at 600 nm with the excitation wavelength at 520 nm using a real-time PCR instrument (StepOnePlus, Life Technologies, Singapore). The samples were held at 10 °C for 10 min and then heated to 95 °C at a heating rate of 1 °C/min. The melting temperature ( $T_m$ ) values of the complexes were calculated by obtaining the main peak value from derivative melting curves, which are the first derivatives of the original fluorescence diagram.

### 2.4 Gel electrophoresis analysis

Different volumes (3 μL, 2 μL, 1 μL, 0.5 μL, 0.25 μL, and 0.1 μL) of a 20-bp DNA marker (100 μg/mL) were separately loaded in a 10% polyacrylamide gel (with TAE buffer) and stained with 1 × GelRed in 1 × TAE buffer for 20 min. Electrophoresis was carried out in 1 × TAE buffer under 120 V for 1 h.

### 3 Results and discussion

#### 3.1 Dyeing mechanism of GelRed

Figure 1a shows the chemical structures of EtBr and GelRed, respectively [40]. GelRed can be regarded as a dimeric EtBr (with  $\text{Br}^-$  replaced by  $\text{I}^-$ ) connected by a hydrocarbon linkage, which has been proven to be a bis-intercalator [23, 40, 41, 45]. The schematic in Fig. 1b illustrates the possible manner of its intercalation into a DNA double helix.

#### 3.2 Fluorescence quantification of dsDNA

First, we tested the capability of GelRed to quantify DNA structures. Here we used the 20-bp DNA ladder as the sample, which can be regarded as a mixture of dsDNAs of varying lengths (ranging from 20 to 500 bp). We conducted electrophoresis with a gel loaded with different quantities of the sample. The resulting image (Fig. 2a) shows that along with the decline of DNA quantity (from left to right, 300 ng, 200 ng, 100 ng, 50 ng, 25 ng, and 12.5 ng), the fluorescence intensity dropped correspondingly. We quantified the band intensity from the gel image (Fig. 2b) and found that it linearly correlated to the quantity of DNA (Fig. 2c). The linear regression function is  $y = 141.5x - 10.9$  ( $R^2 = 0.995$ ), where  $y$  is the fluorescence intensity (arbitrary unit, or a.u.) obtained from the gel bands and  $x$  is the quantity of DNA. These results indicate that the amount of dsDNA structures can be well quantified by measuring their GelRed fluorescence intensity.

#### 3.3 Discrimination of different DNA structures with GelRed

We investigated the fluorescence variations among different DNA structures. We designed two ssDNAs with the

same length (20 nt) but of different sequences. According to the predictions from NUPACK, one of them can form a self-folded secondary structure (referred to as stem-loop ssDNA, with predicted Gibbs free energy change  $\Delta G = -3.83$  kcal/mol, under 25 °C) and the other cannot (referred to as linear ssDNA). The fluorescence spectroscopic measurements (Fig. 3a) showed that the GelRed-stained stem-loop ssDNA showed  $\sim 4.8$ -fold stronger fluorescence compared to the linear one of equal concentration. Meanwhile, the dsDNA of equal length and molar concentration showed much stronger fluorescence compared to both ssDNAs ( $\sim 3.4$ -fold stronger than that of the stem-loop ssDNA and  $\sim 16.3$ -fold stronger than that of the linear ssDNA). Considering these results and the mechanism of GelRed staining, we can deduce that DNA structures with more paired bases can be intercalated with more GelRed molecules, thus showing stronger fluorescence. Here, the fully complementary dsDNA has 20 paired bases, the stem-loop ssDNA has 3 paired bases according to the prediction, and the linear ssDNA has no paired bases; their fluorescence intensities indeed matched this relationship. Therefore, for different DNA structures of equal molar concentration, GelRed can be used as an indicator for the extent of base pairing in DNA intramolecular self-folding or intermolecular hybridization.

We then asked whether GelRed has a bias for the base pair compositions of dsDNAs. We synthesized four dsDNAs (ds1–4) that were 20 bp but had different GC contents (0%, 15%, 30%, and 50%, respectively, as listed in Fig. 3b). As we know, a G–C base pair comprises three hydrogen bonds and is thus more thermostable than an A–T base pair with two hydrogen bonds. The fluorescence measurements (Fig. 3b) revealed that the dsDNAs with higher GC content showed higher GelRed fluorescence intensity. The dsDNA with a GC content of 50% (ds4) gave a  $\sim$  threefold higher fluorescence intensity compared to that without a G–C base (ds1). We hypothesize that this is because high GC content leads to a more

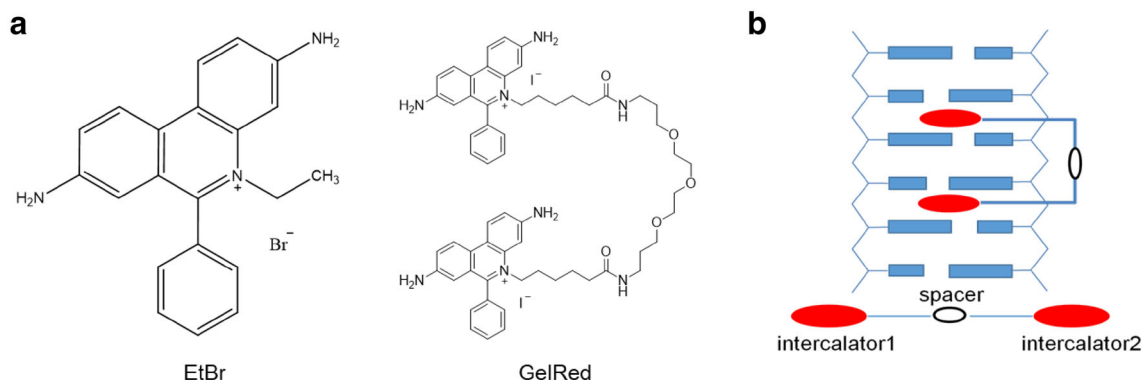


**Fig. 1** a Chemical structure of EtBr (left) and GelRed (right). b Schematics of the intercalation of GelRed into the DNA double helix (Color online)

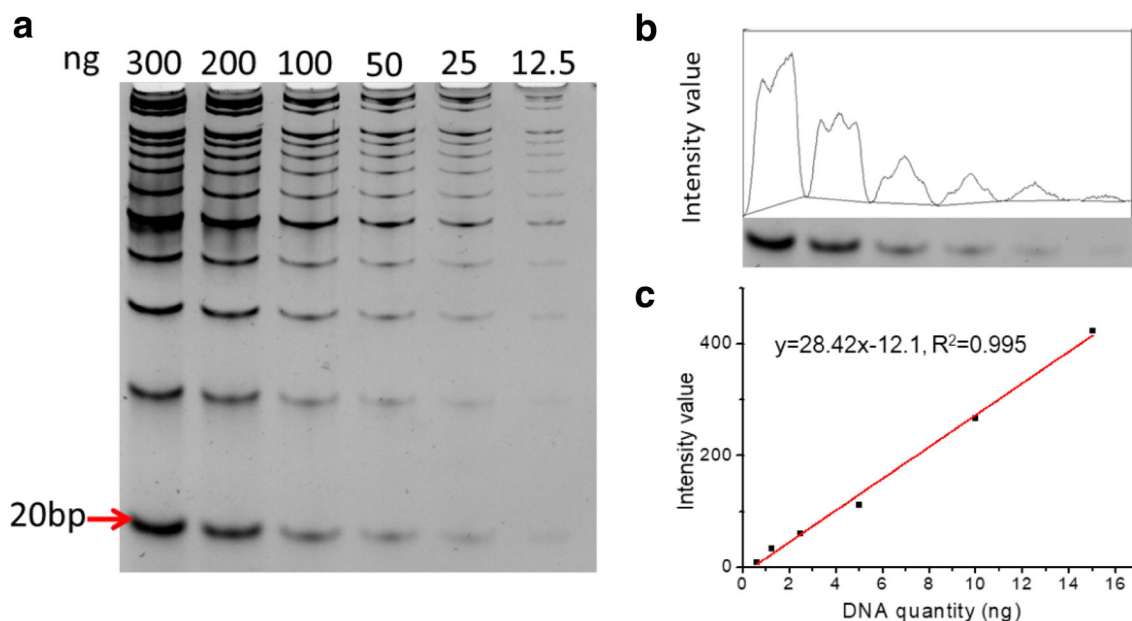


**Fig. 2** **a** Polyacrylamide gel electrophoresis of 20-bp DNA marker (from left to right, 300 ng, 200 ng, 100 ng, 50 ng, 25 ng, and 12.5 ng, respectively, loaded in a 10% polyacrylamide TAE gel and stained with 1 × GelRed in 1 × TAE buffer for 20 min). **b** Fluorescence

intensities quantified from the 20-bp bands of different quantities. **c** Linear regression of fluorescence intensity versus the quantity of the 20-bp DNA

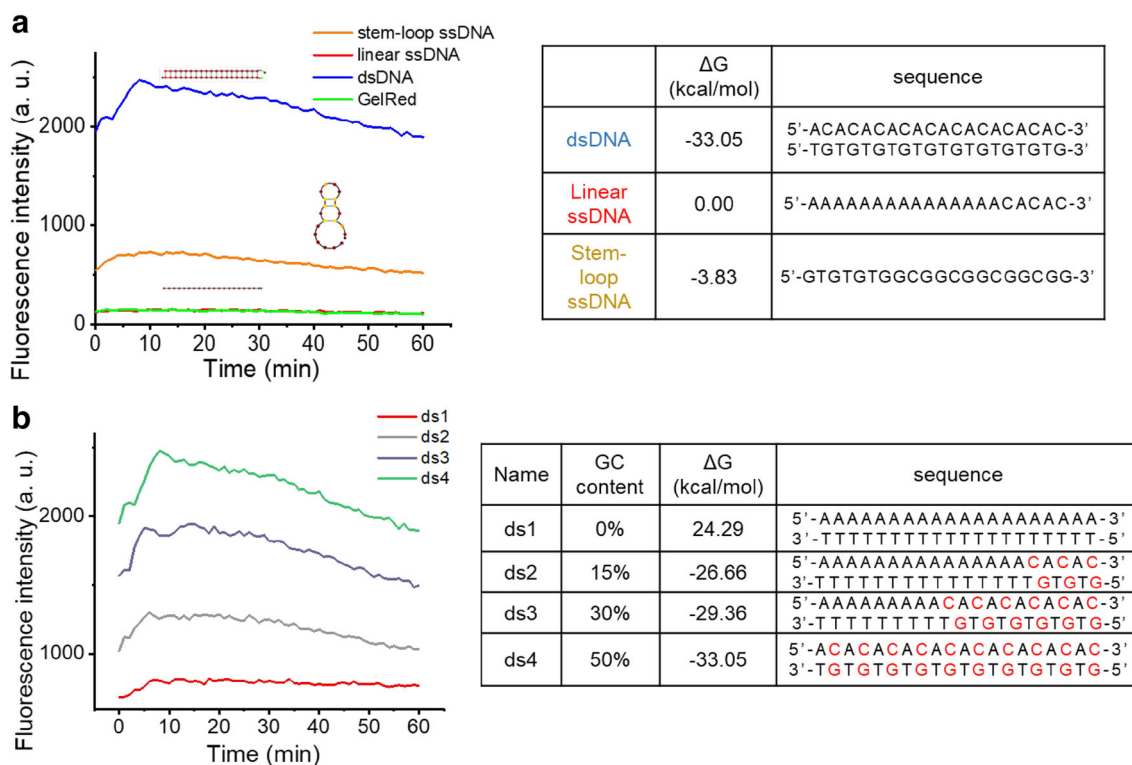
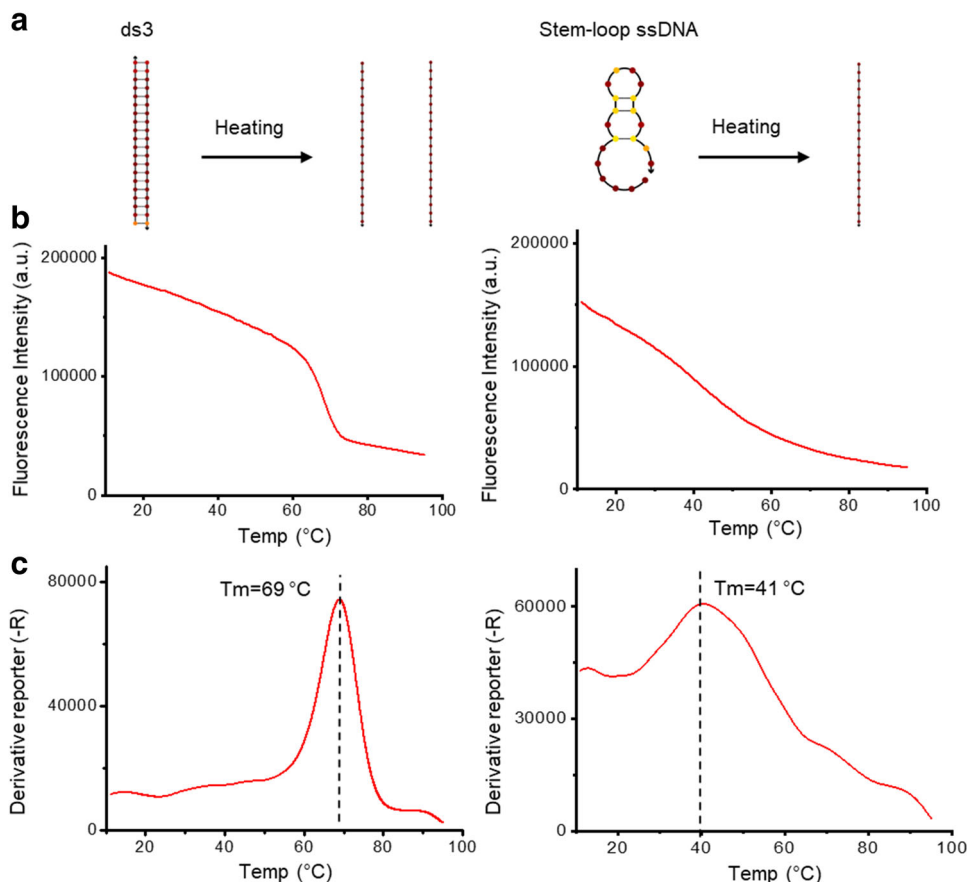


**Fig. 3** Fluorescence spectrograms of GelRed-stained **a** stem-loop ssDNA; **b** dsDNAs. Concentration, 1  $\mu$ M. Tables (right panel): the sequences and  $\Delta G$  (predicted by NUPACK) of the DNA structures (Color online)

thermostable double-helix structure, and thus benefits the intercalation of GelRed molecules. Based on the above results, we can conclude that the fluorescence intensity of a

GelRed-stained DNA structure has a correlation to the thermostability of its secondary structure (including ssDNA self-folding or dsDNA base pairing). This

**Fig. 4** **a** Schematic of temperature-dependent conformational transformation of the dsDNA (ds3) and the stem-loop ssDNA. **b** Temperature-dependent GelRed fluorescence dynamics of ds3 and the stem-loop ssDNA. **c** Derivative melting curves indicating melting temperatures ( $T_m$ ) of ds3 and the stem-loop ssDNA (Color online)



thermostability can be quantified in the form of Gibbs free energy change ( $\Delta G$ ) from the linear ssDNAs to the resulting secondary structures or dsDNAs. In our study, DNA structures with more negative  $\Delta G$  (more thermostable) indeed showed stronger GelRed fluorescence, which supported this hypothesis. We further analyzed the fluorescence of the component ssDNAs of the four dsDNAs that have different sequences (no predicted secondary structures, predicted  $\Delta G = 0$ ). Based on the results (Fig. S1 in Supporting Information), they all showed negligible fluorescence regardless of their sequence, suggesting that the fluorescence intensity is indeed determined by paired bases (thermostability), rather than by different DNA sequences.

Next, we compared the fluorescence resulting from EtBr and GelRed staining. According to the results (Fig. S2 in Supporting Information), the GelRed-stained ds4 structure exhibited  $\sim 14$ -fold stronger fluorescence compared to linear ssDNAs, while the EtBr-stained ds4 structure showed only  $\sim 7$ -fold fluorescence enhancement, indicating that GelRed leads to higher resolution in discriminating different DNA structures. Moreover, considering that EtBr has proven to be mutagenic in Ames tests, GelRed would be a good alternative.

To test the stability and selectivity of GelRed toward DNA in physiological environments, we incubated DNA structures with GelRed in cell culture media minimum essential medium (MEM) containing 10% (v/v) fetal bovine serum (FBS). By comparing their fluorescence spectra (Fig. S3 in Supporting Information), we found the correlation between GelRed fluorescence intensity and DNA structures was not severely interfered with, suggesting the potential of GelRed to deal with real biological samples.

### 3.4 Real-time monitoring of DNA conformational transformations

Having established the correlation between structural thermostability and GelRed fluorescence, we further demonstrated the use of GelRed in real-time monitoring of DNA conformational changes upon cyclic temperature variations. Here, we treated the GelRed-stained DNA structures with controlled temperature changes and recorded the temperature-dependent dynamics of the fluorescence intensity using a real-time quantitative thermocycler. As the temperature rose, the dsDNA structure (ds4) and the stem-loop ssDNA structure were expected to transform into linear strands (Fig. 4a). The observation (Fig. 4b) showed

that, along with the rising temperature, the fluorescence intensity of both structures decreased. When the temperature passed a certain point, the fluorescence dropped more steeply, suggesting the melting of the secondary structures. Therefore, by derivation, we obtained the melting curves (Fig. 4c) of both structures. The main peaks of the melting curves indicated that the measured melting temperature ( $T_m$ ) of ds3 is  $\sim 69$  °C, while the  $T_m$  of the stem-loop ssDNA structure is  $\sim 41$  °C. The results were close to those measured using SYBR Green I (71 °C and 42 °C, respectively, see Table S1 in Supporting Information), another widely used intercalating dye for quantitative thermostability analysis of nucleic acids [46]. These results indicate that GelRed fluorescence can sensitively respond to the conformational changes of DNA structures in a real-time and label-free manner, which shows promise for biological research and DNA nanotechnology.

## 4 Conclusion

In this study, we used an intercalating dye, GelRed, to characterize different DNA structures, including ssDNAs with or without secondary structures and dsDNAs with different base compositions. We showed that GelRed can help discriminate these structures in a quantitative manner. We found that the fluorescence intensity of a GelRed-stained DNA structure is positively correlated to the thermostability (or Gibbs free energy change) of its secondary structure. More thermostable secondary structures (e.g., ssDNAs with stem-loop structures or dsDNAs with higher GC contents) lead to stronger fluorescence intensities. We also demonstrated that by using GelRed, the dynamics of DNA conformational changes can be monitored in real time. In future studies, we will further explore the use of GelRed in investigating other important nucleic acid structures (e.g., chromatin or G-quadruplex) [47]. We also envision that the combination of GelRed with advanced characterizing technologies (e.g., temperature-gradient circular dichroism analysis [48] or high-resolution melting techniques [49]) may help facilitate studies on more complex nucleic acid structures.

## References

- G.L. Li, X.A. Ruan, R.K. Auerbach et al., Extensive promoter-centered chromatin interactions provide a topological basis for transcription regulation. *Cell* **148**, 84–98 (2012). <https://doi.org/10.1016/j.cell.2011.12.014>
- W.L. Deng, J.W. Rupon, I. Krivega et al., Reactivation of developmentally silenced globin genes by forced chromatin looping. *Cell* **158**, 849–860 (2014). <https://doi.org/10.1016/j.cell.2014.05.050>
- E. Splinter, E. de Wit, E.P. Nora et al., The inactive X chromosome adopts a unique three-dimensional conformation that is dependent on Xist RNA. *Genes Dev.* **25**, 1371–1383 (2011). <https://doi.org/10.1101/gad.633311>
- B. He, C.Y. Chen, L. Teng et al., Global view of enhancer-promoter interactome in human cells. *Proc. Natl. Acad. Sci. U.S.A.* **111**, E2191–E2199 (2014). <https://doi.org/10.1073/pnas.1320308111>
- Z.S. Gao, S.H. Deng, J. Li et al., Sub-diffraction-limit cell imaging using a super-resolution microscope with simplified pulse synchronization. *Sci. China Chem.* **60**, 1305–1309 (2017). <https://doi.org/10.1007/s11426-016-9028-5>
- S.P. Wang, S.H. Deng, X.Q. Cai et al., Superresolution imaging of telomeres with continuous wave stimulated emission depletion (STED) microscope. *Sci. China Chem.* **59**, 1519–1524 (2016). <https://doi.org/10.1007/s11426-016-0020-9>
- J. Li, A.A. Green, H. Yan et al., Engineering nucleic acid structures for programmable molecular circuitry and intracellular biocomputation. *Nat. Chem.* **9**, 1056–1067 (2017). <https://doi.org/10.1038/nchem.2852>
- X.H. Mao, A.J. Simon, H. Pei et al., Activity modulation and allosteric control of a scaffolded DNzyme using a dynamic DNA nanostructure. *Chem. Sci.* **7**, 1200–1204 (2016). <https://doi.org/10.1039/c5sc03705k>
- H. Pei, X.L. Zuo, D. Zhu et al., Functional DNA nanostructures for theranostic applications. *Acc. Chem. Res.* **47**, 550–559 (2014). <https://doi.org/10.1021/ar400195t>
- Y. Zhao, F. Li, L.J. Guo et al., The nuclei imaging of nucleus localization signal-DNA tetrahedron composite nanostructures. *Nucl. Sci. Technol.* **40**, 48–53 (2017). <https://doi.org/10.11889/j.0253-3219.2017.hjs.40.050501>
- P. Chen, D. Pan, C.H. Fan et al., Gold nanoparticles for high-throughput genotyping of long-range haplotypes. *Nat. Nanotechnol.* **6**, 639–644 (2011). <https://doi.org/10.1038/Nnano.2011.141>
- H. Pei, L. Liang, G.B. Yao et al., Reconfigurable three-dimensional DNA nanostructures for the construction of intracellular logic sensors. *Angew. Chem. Int. Ed.* **51**, 9020–9024 (2012). <https://doi.org/10.1002/anie.201202356>
- Z.L. Ge, H. Pei, L.H. Wang et al., Electrochemical single nucleotide polymorphisms genotyping on surface immobilized three-dimensional branched DNA nanostructure. *Sci. China Chem.* **54**, 1273–1276 (2011). <https://doi.org/10.1007/s11426-011-4327-6>
- F. Yang, X.L. Zuo, Z.H. Li et al., A bubble-mediated intelligent microscale electrochemical device for single-step quantitative bioassays. *Adv. Mater.* **26**, 4671–4676 (2014). <https://doi.org/10.1002/adma.201400451>
- G.B. Yao, J. Li, J. Chao et al., Gold-nanoparticle-mediated jigsaw-puzzle-like assembly of supersized plasmonic DNA origami. *Angew. Chem. Int. Ed.* **54**, 2966–2969 (2015). <https://doi.org/10.1002/anie.201410895>
- D.K. Ye, X.L. Zuo, C.H. Fan, DNA nanostructure-based engineering of the biosensing interface for biomolecular detection. *Prog. Chem.* **29**, 36–46 (2017). <https://doi.org/10.7536/Pc161214>
- Y. Hori, N. Otomura, A. Nishida et al., Synthetic-molecule/protein hybrid probe with fluorogenic switch for live-cell imaging of DNA methylation. *J. Am. Chem. Soc.* **140**, 1686–1690 (2018). <https://doi.org/10.1021/jacs.7b09713>
- J.B. Liu, C. Yang, C.N. Ko et al., A long lifetime iridium(III) complex as a sensitive luminescent probe for bisulfite detection in living zebrafish. *Sens. Actuators B Chem.* **243**, 971–976 (2017). <https://doi.org/10.1016/j.snb.2016.12.083>

19. L.J. Liu, W.H. Wang, S.Y. Huang et al., Inhibition of the Ras/Raf interaction and repression of renal cancer xenografts in vivo by an enantiomeric iridium(III) metal-based compound. *Chem. Sci.* **8**, 4756–4763 (2017). <https://doi.org/10.1039/c7sc00311k>
20. K. Vellaisamy, G.D. Li, C.N. Ko et al., Cell imaging of dopamine receptor using agonist labeling iridium(III) complex. *Chem. Sci.* **9**, 1119–1125 (2018). <https://doi.org/10.1039/c7sc04798c>
21. H.M. Wang, Z.Q.Q. Feng, S.J. Del Signore et al., Active probes for imaging membrane dynamics of live cells with high spatial and temporal resolution over extended time scales and areas. *J. Am. Chem. Soc.* **140**, 3505–3509 (2018). <https://doi.org/10.1021/jacs.7b13307>
22. W.H. Wang, K. Vellaisamy, G.D. Li et al., Development of a long-lived luminescence probe for visualizing beta-galactosidase in ovarian carcinoma cells. *Anal. Chem.* **89**, 11679–11684 (2017). <https://doi.org/10.1021/acs.analchem.7b03114>
23. F.A.P. Crisafuli, L.H.M. da Silva, G.M.D. Ferreira et al., Depletion interactions and modulation of DNA-intercalators binding: opposite behavior of the “neutral” polymer poly(ethylene-glycol). *Biopolymers* **105**, 227–233 (2016). <https://doi.org/10.1002/bip.22789>
24. R.M. Clegg, Fluorescence resonance energy-transfer and nucleic acids. *Methods Enzymol.* **211**, 353–388 (1992)
25. M. Masuko, S. Ohuchi, K. Sode et al., Fluorescence resonance energy transfer from pyrene to perylene labels for nucleic acid hybridization assays under homogeneous solution conditions. *Nucleic Acids Res.* (2000). <https://doi.org/10.1093/nar/28.8.e34>
26. W.R. Algar, U.J. Krull, Interfacial transduction of nucleic acid hybridization using immobilized quantum dots as donors in fluorescence resonance energy transfer. *Langmuir* **25**, 633–638 (2009). <https://doi.org/10.1021/la803082f>
27. H. Li, X.E. Fang, H.M. Cao et al., Paper-based fluorescence resonance energy transfer assay for directly detecting nucleic acids and proteins. *Biosens. Bioelectron.* **80**, 79–83 (2016). <https://doi.org/10.1016/j.bios.2015.12.065>
28. I. Konig, A. Zarrine-Afsar, M. Aznauryan et al., Single-molecule spectroscopy of protein conformational dynamics in live eukaryotic cells. *Nat. Methods* **12**, 773 (2015). <https://doi.org/10.1038/Nmeth.3475>
29. M.G. Poirier, E. Oh, H.S. Tims et al., Dynamics and function of compact nucleosome arrays. *Nat. Struct. Mol. Biol.* **16**, 938 (2009). <https://doi.org/10.1038/nsmb.1650>
30. D. Zhu, D.X. Zhao, J.X. Huang et al., Protein-mimicking nanoparticle (Protmin)-based nanosensor for intracellular analysis of metal ions. *Nucl. Sci. Technol.* (2018). <https://doi.org/10.1007/s41365-017-0348-y>
31. Y.H. Wang, Z.J. Wu, Z.H. Liu, Upconversion fluorescence resonance energy transfer biosensor with aromatic polymer nanospheres as the label-free energy acceptor. *Anal. Chem.* **85**, 258–264 (2013). <https://doi.org/10.1021/ac302659b>
32. R. Higuchi, C. Fockler, G. Dollinger et al., Kinetic PCR analysis—real-time monitoring of DNA amplification reactions. *Bio-Technology* **11**, 1026–1030 (1993). <https://doi.org/10.1038/nbt0993-1026>
33. A.M. Haines, S.S. Tobe, H.J. Kobus et al., Properties of nucleic acid staining dyes used in gel electrophoresis. *Electrophoresis* **36**, 941–944 (2015). <https://doi.org/10.1002/elps.201400496>
34. T. Afsar, J.H. Trembley, C.E. Salomon et al., Growth inhibition and apoptosis in cancer cells induced by polyphenolic compounds of *Acacia hydasypica*: involvement of multiple signal transduction pathways. *Sci. Rep.* (2016). <https://doi.org/10.1038/srep23077>
35. M. Mahdavi, K. Pedrood, M. Safavi et al., Synthesis and anti-cancer activity of N-substituted 2-arylquinazolinones bearing trans-stilbene scaffold. *Eur. J. Med. Chem.* **95**, 492–499 (2015). <https://doi.org/10.1016/j.ejmech.2015.03.057>
36. A. Tarushi, S. Perontsis, A.G. Hatzidimitriou et al., Copper(II) complexes with the non-steroidal anti-inflammatory drug tolfenamic acid: structure and biological features. *J. Inorg. Biochem.* **149**, 68–79 (2015). <https://doi.org/10.1016/j.jinorgbio.2015.02.019>
37. J.H. Huang, Z.Y. Wang, J.K. Kim et al., Detecting arbitrary DNA mutations using graphene oxide and ethidium bromide. *Anal. Chem.* **87**, 12254–12261 (2015). <https://doi.org/10.1021/acs.analchem.5b03369>
38. S. Pal, Y.G. Zhang, S.K. Kumar et al., Dynamic tuning of DNA-nanoparticle superlattices by molecular intercalation of double helix. *J. Am. Chem. Soc.* **137**, 4030–4033 (2015). <https://doi.org/10.1021/ja512799d>
39. V.L. Singer, T.E. Lawlor, S. Yue, Comparison of SYBR (R) Green I nucleic acid gel stain mutagenicity and ethidium bromide mutagenicity in the Salmonella/mammalian microsome reverse mutation assay (Ames test). *Mutat. Res., Genet. Toxicol. Environ. Mutagen.* **439**, 37–47 (1999). [https://doi.org/10.1016/S1383-5718\(98\)00172-7](https://doi.org/10.1016/S1383-5718(98)00172-7)
40. F.A.P. Crisafuli, E.B. Ramos, M.S. Rocha, Characterizing the interaction between DNA and GelRed fluorescent stain. *Eur. Biophys. J.* **44**, 1–7 (2015). <https://doi.org/10.1007/s00249-014-0995-4>
41. M. Anjomshoa, M. Torkzadeh-Mahani, Competitive DNA-binding studies between metal complexes and GelRed as a new and safe fluorescent DNA dye. *J. Fluoresc.* **26**, 1505–1510 (2016). <https://doi.org/10.1007/s10895-016-1850-z>
42. X.Q. Li, M. Haroon, S.E. Coleman et al., A simplified procedure for verifying and identifying potato cultivars using multiplex PCR. *Can. J. Plant Sci.* **88**, 583–592 (2008). <https://doi.org/10.4141/Cjps07061>
43. I. Kasajima, N. Ohtsubo, K. Sasaki, Faster, safer, and better DNA purification by ultracentrifugation using GelRed stain and development of mismatch oligo DNA for genome walking. *Biosci. Biotechnol. Biochem.* **78**, 1902–1905 (2014). <https://doi.org/10.1080/09168451.2014.940831>
44. J.Q. Chen, S.F. Xue, Z.H. Chen et al., GelRed/[G(3T)(5)/Tb3 + hybrid: a novel label-free ratiometric fluorescent probe for H<sub>2</sub>O<sub>2</sub> and oxidase-based visual biosensing. *Biosens. Bioelectron.* **100**, 526–532 (2018). <https://doi.org/10.1016/j.bios.2017.09.047>
45. G.J. Atwell, G.M. Stewart, W. Leupin et al., A diacridine derivative that binds by bisintercalation at two contiguous sites on DNA. *J. Am. Chem. Soc.* **107**, 4335–4337 (1985). <https://doi.org/10.1021/ja00300a046>
46. K.M. Ririe, R.P. Rasmussen, C.T. Wittwer, Product differentiation by analysis of DNA melting curves during the polymerase chain reaction. *Anal. Biochem.* **245**, 154–160 (1997). <https://doi.org/10.1006/abio.1996.9916>
47. M.D. Wang, Z.F. Mao, T.S. Kang et al., Conjugating a groove-binding motif to an Ir(III) complex for the enhancement of G-quadruplex probe behavior. *Chem. Sci.* **7**, 2516–2523 (2016). <https://doi.org/10.1039/c6sc00001k>
48. S.C. Lee, T.J. Knowles, V.L.G. Postis et al., A method for detergent-free isolation of membrane proteins in their local lipid environment. *Nat. Protoc.* **11**, 1149–1162 (2016). <https://doi.org/10.1038/nprot.2016.070>
49. T.K. Wojdacz, A. Dobrovic, L.L. Hansen, Methylation-sensitive high-resolution melting. *Nat. Protoc.* **3**, 1903–1908 (2008). <https://doi.org/10.1038/nprot.2008.191>